JNeurosci
THE JOURNAL OF NEUROSCIENCE

Research Articles: Systems/Circuits

Encoding of both reaching and grasping kinematics in dorsal and ventral premotor cortices

Kazutaka Takahashi[1], Matthew D. Best[2], Noah Huh[1], Kevin A. Brown[3], Adil A. Tobaa[1] and Nicholas G. Hatsopoulos[1,2]

[1]*Department of Organismal Biology and Anatomy and*
[2]*Committee on Computational Neuroscience, The University of Chicago, Chicago, IL, 60637*
[3]*Center for Neural Science, New York University, New York, New York, 10003*

DOI: 10.1523/JNEUROSCI.1537-16.2016

Received: 11 May 2016

Revised: 12 December 2016

Accepted: 30 December 2016

Published: 11 January 2017

Author contributions: K.T. and N.G.H. designed research; K.T., M.B., and N.H. performed research; K.T., M.B., N.H., K.A.B., and A.A.T. contributed unpublished reagents/analytic tools; K.T., M.B., N.H., and A.A.T. analyzed data; K.T., M.B., and N.G.H. wrote the paper.

Conflict of Interest: The authors declare no competing financial interests.

This work was supported by grant RO1 NS045853 from the NINDS and RO1 DE023816 from the NIDCR. The authors are grateful for the support of the University of Chicago Research Computing Center for assistance with the calculations carried out in this work. The authors would like to thank Gustavo Alvarez, Alina Scotti, Michelle Guo for assistance in processing motion capture data.

Corresponding Author Information: Kazutaka Takahashi, kazutaka@uchicago.edu, 1025 East 57th St. Culver Rm. 206, Chicago, IL 60637

Cite as: J. Neurosci 2017; 10.1523/JNEUROSCI.1537-16.2016

Encoding of both reaching and grasping kinematics in dorsal and ventral premotor cortices

Kazutaka Takahashi[1*], Matthew D. Best[2], Noah Huh[1], Kevin A. Brown[3], Adil A. Tobaa[1], and Nicholas G. Hatsopoulos[1,2]

1. Department of Organismal Biology and Anatomy and 2. Committee on Computational Neuroscience, The University of Chicago, Chicago, IL, 60637
3. Center for Neural Science, New York University, New York, New York, 10003

*Corresponding Author Information:
Kazutaka Takahashi
kazutaka@uchicago.edu
1025 East 57th St.
Culver Rm. 206
Chicago, IL 60637

Number of pages: 38
Number of figures: 10
Number of tables: 2
Number of words (total): 9763
Number of words (abstract): 222
Number of words (introduction): 489/650
Number of words (discussion): 1754/1500

Acknowledgements
This work was supported by grant RO1 NS045853 from the NINDS and RO1 DE023816 from the NIDCR. The authors are grateful for the support of the University of Chicago Research Computing Center for assistance with the calculations carried out in this work. The authors would like to thank Gustavo Alvarez, Alina Scotti, Michelle Guo for assistance in processing motion capture data. The authors declare no competing financial interests.

Abstract

Classically, it has been hypothesized that reach-to-grasp movements arise from two discrete parieto-frontal cortical networks. As part of these networks, the dorsal premotor cortex has been implicated in the control of reaching movements of the arm, while the ventral premotor cortex has been associated with the control of grasping movements of the hand. Recent studies have shown that such a strict delineation of function along anatomical boundaries is unlikely partly because reaching to different locations can alter distal hand kinematics and grasping different objects can affect kinematics of the proximal arm; Here, we used chronically implanted multi-electrode arrays to record unit spiking activity in both PMd and PMv simultaneously while rhesus macaques engaged in a reach-to-grasp task. Generalized linear models were used to predict the spiking activity of cells in both areas as a function of different kinematic parameters, as well as spike history. To account for the influence of reaching on hand kinematics and vice-versa, we applied demixed principal component analysis to define kinematics synergies that maximized variance across either different object locations or grip types. We found that single cells in both PMd and PMv encode the kinematics of both reaching and grasping synergies suggesting that this classical division of reach and grasp in PMd and PMv, respectively, does not accurately reflect the encoding preferences of cells in those areas.

Significance statement

For reach-to-grasp movements, the dorsal premotor cortex (PMd) has been implicated in the control of reaching movements of the arm, while the ventral premotor cortex (PMv) has been associated with the control of grasping movements of the hand. We recorded unit spiking activity in PMd and PMv simultaneously while macaques performed a reach-to-grasp task. We modeled the spiking activity of neurons as a function of kinematic parameters and spike history. We applied demixed principal component analysis to define kinematics synergies. We found that single units in both PMd and PMv encode the kinematics of both reaching and grasping synergies suggesting that the division of reach and grasp in PMd and PMv, respectively, can't be made based on their encoding properties.

Introduction

Reaching to grasp is a fundamental, ethologically relevant primate behavior (Kaas et al., 2013). Several cortical and sub-cortical structures are involved in the generation of these movements (Fattori et al., 2004; Grafton, 2010; Kaas et al., 2013). Recently, much emphasis has been placed on understanding the behavior of single cells in primary motor cortex (MI), one of the main sources of cortical output to the spinal cord, during reach to grasp movements (Saleh et al., 2010, 2012, Mollazadeh et al., 2011, 2014). The motor cortex, however, does not exhibit a clear hierarchical organization with MI as the sole source of corticospinal output (He et al., 1993; Dum and Strick, 2005). Rather, MI is part of a network of cortical areas involved in the production of reach to grasp movements. Two other cortical areas that are densely

75 connected horizontally with MI are dorsal and ventral premotor cortex (PMd and PMv,
76 respectively) with these two areas providing a large proportion of cortical inputs to MI
77 (Dum and Strick, 2005; Dea et al., 2016).

78 The dual channels hypothesis has posited that reach to grasp movements arise
79 from the temporal coordination of activity in independent reaching and grasping brain
80 networks (Jeannerod, 1988; Karl and Whishaw, 2013) In this framework, PMd, which
81 makes anatomical connections to superior parietal lobe, specifically area V6A (Fattori et
82 al., 2010, 2012), has been considered part of a dorsomedial parietofrontal reaching
83 network involving movements of the arm, while PMv, which makes anatomical
84 connections to inferior parietal lobe, specifically AIP and VIP (Luppino et al., 1999;
85 Borra et al., 2008), has been associated with a dorsolateral parietofrontal grasping
86 network and concerned with distal aspects of the limb, namely, the hand (Dum and
87 Strick, 2005; Hoshi and Tanji, 2007; Grafton, 2010; Dea et al., 2016). However, PM
88 single unit spiking activities have been shown to encode both grip type and target
89 position/reach direction during reach-to-grasp movements in both PMd and PMv
90 (Lehmann and Scherberger, 2013; Stark et al., 2007). Those studies considered grip
91 type and target position/reach direction as categorical variables. What is unknown is
92 whether the encoding of kinematic trajectories of reaching and grasping is spatially
93 segregated across the premotor cortex.

94 Here, we directly tested whether representations of reaching and grasping
95 kinematics were strictly segregated in PMd and PMv. To address this, however, we had
96 to account for the fact that reaching for objects in different locations influenced not only
97 proximal limb kinematics of the arm but also distal kinematics of the hand. Likewise,

grasping different objects affected both hand and arm kinematics. Thus, we applied a novel dimensionality reduction technique to dissociate anatomical representations (i.e. based on encoding specific joints) from functional representations (i.e. encoding reach-related or grasp-related kinematic synergies). We found no evidence of a strict segregation of reaching and grasping activity in PMd or PMv. Instead, we observed that both areas contained complete anatomical representations of the upper limb and functional representations of both reaching and grasping.

Methods

Neurophysiology

All surgical and experimental procedures were approved by the University of Chicago Animal Care and Use Committee and conformed to the principles outlined in the Guide for the Care and Use of Laboratory Animals (NIH publication no 86-23 revised 1985). Two rhesus macaques (*macaca mulatta*) were implanted with 96-electrode Utah arrays in the dorsal and ventral premotor cortex contralateral to their working arm. Electrodes were 1.5 mm in length except for the array in PMd of animal J (1.0 mm). Neural spiking activity from the electrodes were amplified with a gain of 5000, band-pass filtered between 0.3 Hz and 7.5 kHz, and recorded digitally (14 bit resolution) using a Cerebus acquisition system (Blackrock Microsystems, Salt Lake City, UT). A threshold was set above the noise floor on each channel (5.5 standard deviations) and every time this threshold was crossed a 1.6 ms sample (sampled at 30 kHz) was recorded as a putative spike waveform. These threshold crossings were subsequently sorted offline using a semi-manual clustering procedure (Offline Sorter, Plexon Inc., Dallas, TX, RRID:SCR_000012). Only sorted waveforms with a signal-to-

noise ratio (SNR) greater than 3 were used in subsequent analyses. Here, signal to noise ratio is defined as the peak minus the trough of the average waveform divided by the average standard deviation of the waveform across time.

Behavioral Task

Two male rhesus macaques were trained to perform a reach to grasp task with their left hand while their heads were fixed. A robot (RV-1A-S11 6-axis robot; rixan.com) presented each animal with objects (Fig. 1A) to grasp at four different spatial locations (Fig. 1B) in its peripersonal space. The set of objects consisted of geometric shapes that were designed to evoke a variety of different hand conformations when grasped. Object and location pairings were randomly varied on a trial-by-trial basis to minimize the amount of motor planning. Additionally, the animal's vision was occluded between trials with a pneumatically controlled screen. Once the vision screen was opened, the animal made a reach to grasp movement to the target and held his grip for at least 500 ms in order to receive a juice reward. During each movement, the animal was able to see his arm and hand. Each object was attached to a shaft whose ending was attached to a cube with a magnet that allowed the experimenter to quickly affix a different object to the end-effector of the robot on each trial.

The precise set of objects that were presented to animal L consisted of 5 different objects (Cylinder, Small Disc, Key, Large Disc, Ring) in different orientations for a total of 11 different grasp conformations, or grips, (Cylinder Horizontal, Cylinder Out, Cylinder Vertical, Small Disc Horizontal, Small Disc Out, Small Disc Vertical, Key, Large Disc Horizontal, Large Disc Vertical, Ring Horizontal, Ring Vertical). On average, the animal completed 21 repetitions of each grip/location pairing, although some

combinations were less frequent than others due to the random sampling of objects, with the minimum number of repetitions being 5. Animal J was presented with three objects (Cylinder, Small Disc, Ring) to evoke four different grips (Cylinder Out, Small Disc Out, Ring Horizontal, Ring Vertical). On average, animal J completed 36 repetitions of each grip/location pairing, and all combinations were sampled at least 15 times. Data from each monkey was recorded from one session each.

Motion capture and inverse kinematics

A 10-camera motion capture system (Vicon Motion Tracking System, Oxford, UK) detected and recorded the 3-D position of retro reflective markers glued to the animal. A total of 30 markers were placed on the animal's dorsal hand and dorsolateral arm enabling the tracking of 21 degrees of freedom in the arm and hand (listed below). The motion capture system was also used to monitor the position of the object and vision block screen. The time series of 3D marker positions were lowpass filtered bi-directionally (4^{th} order Butterworth filter 15 Hz cutoff). All filtering and calculations are done in Matlab (Mathworks, Natick, MA, RRID:SCR_001622) unless otherwise noted. To measure grasp aperture, we computed the Euclidean distance between markers attached to the distal most aspects of the thumb, and index finger (D1 and D2, respectively).

To compute wrist speed, we numerically differentiated the positional data of three markers on the animal's wrist. After numerical differentiation, wrist velocities were again lowpass filtered (using the same filter design as before). Wrist speed was defined as the average tangential velocity of the three wrist markers. Movement onset, derived from wrist speed, was defined as the first moment that wrist speed exceeded 10% of the

maximum wrist speed. Reaction times were subsequently defined as the difference in time between movement onset and release of the vision block.

We used open-source software (Delp et al., 2007, Opensim, RRID:SCR_002683) to infer joint angles from marker positional data. We estimated joint angles for 21 degrees of freedom in the arm and hand including: humerus flexion/extension, humerus abduction/adduction, humerus rotation, elbow flexion/extension, wrist pronation/supination, wrist abduction/adduction, wrist flexion/extension, 1 carpal-metacarpal (CMC) flexion/extension, 1 CMC abduction/adduction, 1 metacarpal-phalangeal (MCP) flexion/extension, 1 MCP abduction/adduction, 2 MCP abduction/adduction, 2 MCP flexion/extension, 2 proximal interphalangeal (PIP) flexion/extension, 3 MCP flexion/extension, 3 MCP abduction/adduction, 4 MCP flexion/extension, 4 MCP abduction/adduction, 4 PIP flexion/extension, 5 MCP flexion/extension, 5 MCP abduction/adduction, and 5 CMC flexion/extension,. Inverse kinematics was bi-directionally, lowpass filtered with a 6 Hz cutoff.

Demixed principal components analysis

We used a novel dimensionality reduction technique, demixed principal component analysis (dPCA), to identify kinematic synergies associated with reaching, grasping, the interaction of reach and grasp, or synergies that were common across all experimental conditions (Brendel et al., 2011; Kobak et al., 2016). This analysis was motivated by two observations about the kinematics. First, on a given trial, there are often strong correlations between the kinematics of different joints suggesting that most of the variance in the kinematics may be described by a few kinematic synergies, often estimated using principal component analysis (Santello and Soechting, 1998; Mason et

190 al., 2001). Second, the correlation patterns across joints during reach-to-grasp
191 movements depend upon the exact nature of the movement; thus, different
192 experimental conditions may produce different correlation patterns (Todorov and
193 Ghahramani, 2004). Briefly, the dPCA algorithm attempts to find linear combinations of
194 kinematic variables that explain the most variance, yet also vary only with a given
195 experimental condition.

196 We present a mathematical explanation of dPCA that closely mirrors the
197 description in (Kobak et al., 2016). Suppose that every trial, *e* (of *E* total trials), has an
198 associated location, *l* (out of *L* possible locations), and grip *o* (out of *O* possible grips).
199 Also, suppose that on every trial we have recorded the activity of *J* kinematic features at
200 *T* different time points. We computed the trial-average kinematic trajectory of every
201 kinematic feature, *j*, for each grip and location pairing denoted $R_{jlo}(t)$. We then gathered
202 all the trial-averaged kinematic trajectories into a single matrix, $\boldsymbol{X}$ of size *J* x *LOT*. We
203 subsequently demeaned $\boldsymbol{X}$ such that the average of any kinematic feature over all
204 locations, grips, and times was 0. It has been previously shown that for such a matrix,
205 $\boldsymbol{X}$, it can be decomposed into independent parts called marginalizations that satisfy:

$$\boldsymbol{X} = \boldsymbol{X}_t + \boldsymbol{X}_{tl} + \boldsymbol{X}_{to} + \boldsymbol{X}_{lto},$$

206 where $\boldsymbol{X}_t$ denotes the time varying, but location and grip-invariant part of $\boldsymbol{X}$, obtained by
207 averaging $\boldsymbol{X}$ over all locations and grips, i.e.,

$$\boldsymbol{X}_t = \frac{1}{LO}\sum_{l=1}^{L}\sum_{o=1}^{O}\boldsymbol{X}_{\boldsymbol{tlo}.}$$

208 The location dependent term, $\boldsymbol{X}_{tl}$, is obtained by averaging $\boldsymbol{X} - \boldsymbol{X}_t$ over all grips, and
209 similarly, the grip dependent term, $\boldsymbol{X}_{to}$ is obtained by averaging $\boldsymbol{X} - \boldsymbol{X}_t$ over all locations.
210 Finally, the location-grip interaction, $\boldsymbol{X}_{lto}$ is obtained by computing $\boldsymbol{X}_{lto} = \boldsymbol{X} - \boldsymbol{X}_t - \boldsymbol{X}_{tl} - \boldsymbol{X}_{to}$.

It is important to note that every marginalization of $\boldsymbol{X}$ has the same dimension as $\boldsymbol{X}$, i.e. J x LOT.

Using the decomposition of $\boldsymbol{X}$ into its marginalizations, dPCA aims to find directions in $\mathbf{R}^J$ that explain as much variance as possible, with the additional constraint that this variance should come from only one marginalization. Unlike standard PCA, dPCA relaxes the assumption that all the directions must be strictly orthogonal. Formulated as a constrained optimization problem, dPCA seeks to find a direction ϕ in $\mathbf{R}^J$, to minimize the following objective:

$$L = \sum_{\phi} \left\| \boldsymbol{X}_{\phi} - F_{\phi} D_{\phi} \boldsymbol{X} \right\|_F^2,$$

where F_{ϕ} is an encoder matrix with q columns, D_{ϕ} is a decoder matrix with q rows, and $||\bullet||^2_F$ denotes the Frobenius norm of a matrix. An efficient algorithm was recently proposed to solve this objective function (Kobak et al., 2016).

In order to compute the cumulative variance explained by the first p dPCs, we cannot simply add variances because the dPCs are not strictly orthogonal. Instead, the cumulative variance explained by the first p dPCs is given by:

$$\frac{\|\boldsymbol{X}\|_F^2 - \left\| \boldsymbol{X} - [f_{1:p}][d_{1:p}]' \boldsymbol{X} \right\|_F^2}{\|\boldsymbol{X}\|_F^2},$$

where $[f_{1:p}]$ is a matrix of the first p encoding vectors, $[d_{1:p}]$ is a matrix of the first p decoding vectors, and $[\bullet]'$ is a transpose of a matrix . We emphasize that the cumulative proportion of variance explained by each component is based off of the trial averaged data in the matrix, $\boldsymbol{X}$.

Generalized linear model analysis

Input features

We attempted to predict the instantaneous probability of spiking in a given single unit from many different combinations of extrinsic covariates (i.e. kinematics and experimental factors) and intrinsic covariates (i.e. neural signals).

Extrinsic covariates

We used the position and velocity of 21 joints in the arm and hand at various time lags as input features to our encoding model. We used 8 different time lags from -156 ms (i.e. spikes lag kinematics by 156 ms) to 208 ms (i.e. spikes lead kinematics by 208 ms) in 52 ms steps. In total, there were 168 (21 joints x 8 lags) positions and velocities for a total of 336 kinematic features. Other extrinsic features included kinematic synergies identified via dPCA. Additional categorical variables indicating the reach location and grip on a given trial were defined; inter-trial intervals were coded as one category in these variables.

Intrinsic covariates

In addition to extrinsic features, intrinsic features such as a given neuron's own spike history and the spike history of other neurons may also contribute to a neuron's firing rate. To account for the fact that spike history may be relevant in different ways at different time scales, we filtered binary spike trains with raised cosine basis functions of the form:

$$y(t) = 0.5\cos(a\log(t+c) - \phi) + 0.5,$$

for *t* such that $a\log(t+c) \in [\phi - \pi, \phi + \pi]$, and 0 elsewhere (Saleh et al., 2012). We specified three different values of φ, the temporal peak of the cosine curve, to account for short (16 ms), medium (44 ms), and long (108 ms) time scale spike history effects.

Each basis vector was convolved with the binary spike train of a given neuron, thus giving rise to 3 spike history vectors for every neuron.

Logistic regression

We used logistic regression to predict the probability that a neuron fired a spike in a small time window (4 ms) based on previously described input features. Mathematically, this model may be expressed as:

$$\log\left[\frac{p_n(t)}{1-p_n(t)}\right] = \beta_0 + \sum_{m=1}^{M}\sum_{k=1}^{K}\beta_{k,m}X_k(t+\tau_m) + \sum_{j=1}^{J}\beta_j X_j(t),$$

where $p_n(t)$ is the probability that neuron n fires a spike at time t, β_0 represents the baseline probability that the cell will spike, $X_k(t-\tau_l)$ is the value of the k^{th} (of K) extrinsic feature at time $t-\tau_m$, where τ_m is the m^{th} (of M) lead or lag time (ranging from 52, 104, and 156 ms leading and 52, 104, 156, 208 ms lagging) against the spike time at t, and $X_j(t)$ is the value of the j^{th} (of J) intrinsic feature at time t with corresponding weights $\beta_{k,m}$ and β_j, respectively.

Data segmentation and assessing goodness of fit

Model goodness of fit (GoF) was quantified using the area under the receiver operating characteristic curve (AUROC) (Hatsopoulos et al., 2007; Saleh et al., 2010, 2012; Truccolo et al., 2010). We assessed goodness of fit using 10 folds of cross-validated test data, and, unless otherwise noted, all reported AUROC values are taken to be the median across cross-validation folds. Each training fold was comprised of at least 329 experimental trials and inter-trial activity between those trials. Because the folds were based on experimental trials rather than data points, the number of test and training

data points varied across folds, however, at least 531,747 and 1,541,496 data points were in every fold in animals J and L, respectively.

Results

The kinematics of unconstrained reaching to grasp

We used a marker-based infrared motion tracking system combined with an advanced biomechanical model of the primate upper limb (Delp et al., 2007) to infer the kinematics of 21 joints in the arm and hand as two rhesus macaques engaged in an unconstrained reach-to-grasp task. We presented multiple grips at different locations in the animal's workspace designed to elicit a diversity of prehensile movements that included both precision and power grips (Fig. 1).

Differences in kinematics across experimental conditions were evident at the level of individual joints (Fig. 2). From visual inspection of Fig. 2A, it can be seen that the different object locations elicited different patterns of arm movement and the different grip types elicited different patterns of hand movement. Less obvious, however, is that the object to be grasped also influenced arm kinematics and, to a lesser extent, the position of the object in space influenced hand kinematics (Fig. 2B). These differences at the level of single joints were also manifested in multi-joint features. The average temporal profiles of grasp apertures were qualitatively different across grips (Fig. 2C) and quantitatively, the maximum grasp aperture over time was significantly different across the four grasping conditions (Kruskal Wallis test, animal J: X^2 with 3 d.f. = 330.84, $p < 0.01$; animal L: X^2 with 3 d.f. 199.91, $p < 0.01$). Similarly, we observed differences in the peak wrist speed across object locations (Kruskal Wallis test, animal J: X^2 with 3 d.f. = 87.16, $p < 0.01$; animal L: X^2 with 3 d.f. 272.19, $p < 0.01$).

To control for the fact that both reaching and grasping affect kinematics in the entirety of the upper limb, we employed a novel dimensionality reduction technique, demixed principal component analysis (dPCA), to identify functionally defined kinematic synergies. Each kinematic synergy (i.e. each dPC) could be either reach-related, grasp-related, condition-independent (i.e. common to all experimental conditions), or an interaction between reach and grasp (i.e. specific to a particular experimental condition). As with other studies that have applied dimensionality reduction techniques to kinematic data (Mason et al., 2001; Mollazadeh et al., 2014; Schaffelhofer et al., 2015), we found that a handful of functional kinematic synergies described the majority of the variability in the kinematics. In both animals, we found 8 components were sufficient to explain 90% of the variance in joint angles (Fig. 3A), while 10 and 9 components were needed to explain 90% of the variance in joint angular velocities in animals J and L, respectively (result not shown). In both animals, we observed that a substantial proportion of the kinematic variance was common across all experimental conditions, and that grasping components explained more variance than reaching components (Fig. 3B). Examples of the kinematic synergies in animal L are shown in Fig. 3C. The temporal evolution of a subset of these kinematic synergies as a function of time relative to the movement onset (MO) is shown in Fig. 4 for both animals. Although the convexity for animal J is flipped, dPC1's for both animals are condition independent and they appear to resemble aperture trajectories and clearly indicate behavioral differences between the two animals: animal J made much faster reaching than animal L. dpc1 CI for animal J appears to represent the invariant hand speed profile. Other grasp or reach specific dPC's show object and location specific components such that trajectories associated

with different locations formed clustered bundles that were distinct for different objects (dPC3 G for animal J and dPC2 G and dPC3 G for animal L), and trajectories associated with different objects formed bundles that were distinct for different locations (dPC4 R for animal J and dPC4 R for animal L).

Encoding of extrinsic features in premotor cortex

One session for each monkey was performed to collect single unit spiking activity from PMd and PMv arrays. We obtained populations of task related units: 51 and 34 units from PMd and PMv respectively for monkey J and 29 and 22 for monkey L respectively. Figure 5 illustrates one example each for PMd and PMv single unit activities across different objects and different locations.

We used generalized linear models (GLM) to develop encoding models of premotor cortical single unit activity and compared the performance of these models that explicitly accounted for the moment-by-moment kinematic features against a more abstract, set-related representation of behavior. In this first class of model, we used the detailed kinematics of 21 joints in the arm and hand at a variety of different time lags to predict spiking activity (see Methods for details). In contrast, the second class of model, the set-related model, assumed a single, constant firing rate for each experimental condition. To assess model performance, the area under the receiver operating characteristic curve (AUROC) was computed for each model.

Across all animals, brain areas, and types of model, we found that the median AUROC values across cells were significantly greater than the chance level of the AUROC, 0.5 (Fig. 6A; Wilcoxon signed rank test, all $p < 0.01$). In both animals, we observed that kinematics better predicted activity in PMd as compared to PMv (Fig. 6A;

Mann-Whitney *U*-test, animal J: $Z = 2.85$, $p < 0.004$; animal L: $Z = 4.12$, $p < 0.01$). The set related models also predicted activity in PMd better than PMv in animal L (Fig. 6A; $Z = 4.75$, $p < 0.01$) but not in animal J ($Z = 1.59$, $p > 0.05$). In both animals and brain areas, we found that encoding models based on kinematics better predicted spiking activity than the set-related models (Fig. 6B; Wilcoxon signed rank test, animal J PMd: $Z = 5.74$, $p < 0.01$; PMv: $Z = 4.98$, $p < 0.01$; animal L PMd: $Z = 3.45$, $p < 0.01$; PMv: $Z = 4.11$, $p < 0.01$). We computed AUROC for each kinematic lead/lag, but there was no clear indication of an optimal lead/lag time for either of the two cortical areas (results now shown).

Having established that whole arm kinematics were predictive of spiking activity in PMd and PMv, we subsequently considered which aspects of the kinematics were important. The dual channels hypothesis posits that PMd is concerned with the proximal aspect of the limb while PMv is related to the distal aspect. We tested the extent to which anatomical segments of the limb were represented in both areas. Encoding models were fit using only arm kinematics, (i.e. shoulder and elbow kinematics), or only hand kinematics (i.e. wrist and fingers). We found evidence that both arm and hand kinematics were predictive of spiking in each area as the median AUROC across neurons was significantly greater than 0.5 (Fig. 7A; Wilcoxon signed rank test, all $p < 0.01$). But, this finding, in isolation, does not provide strong evidence against the dual channels hypothesis. For example, a cell that truly encodes only arm kinematics may appear to also encode hand kinematics simply because of correlations between arm and hand kinematics.

We performed a control analysis to ensure that any putative encoding relationship was not a product of kinematic correlations. In this analysis, we subtracted off either arm or hand AUROC from the AUROC of the full model containing both arm and hand kinematics (Fig. 7B). Returning to the previous example, if a cell encodes only arm kinematics, then the difference between the full model AUROC and the arm AUROC should be 0. However, the difference between the full model AUROC and the hand AUROC should be positive because this example cell truly encodes arm kinematics, which the full model contains. In real data, cells that had a positive difference between full model AUROC and hand model AUROC were classified as encoding arm kinematics. Similarly, cells with positive differences between full model AUROC and arm model AUROC were classified as encoding hand kinematics. These classifications were not mutually exclusive. We found that both arm and hand kinematics were effective predictors of single premotor cortical neuron activity. We observed (Table 1) that 82% PMd and 79% PMv cells for monkey J and 100% PMd and 95% PMv cells for monkey L encoded arm kinematics, 56% PMd and 53% PMv cells for monkey J and 75% PMd and 76% PMv cells for monkey L encoded hand kinematics, while 42% PMd and 41% PMv cells for monkey J and 75% PMd and 71% PMv cells for monkey L encoded both arm and hand kinematics respectively. The dual channels hypothesis would predict that cells encode either arm kinematics or hand kinematics, i.e., that they were anti-correlated. However, the proportion of cells that encoded both arm and hand kinematics simultaneously was not significantly different than would be expected if both arm and hand kinematics were encoded statistically independently

(binomial test, B0.497, 121 = 62, p > 0.05), i.e., the presence of encoded arm kinematics does not affect the encoding of hand kinematics and vice verse.

We subsequently tested whether the arm and hand were preferentially represented in PMd and PMv, respectively by subtracting the AUROC of the hand-only from the arm-only models. We found that arm kinematics was preferentially represented in the PMd of both animals because the median AUROC differences were significantly greater than 0 (Fig. 7C; Wilcoxon signed rank test, animal J: $Z = 2.51$, $p < 0.02$; L: $Z = 3.35$, $p < 0.01$). Arm kinematics was also preferentially represented in the PMv of animal J ($Z = 2.57$, $p < 0.01$), but not in animal L ($Z = -0.41$, $p > 0.05$).

In the previous analysis, we showed that both PMd and PMv encode both arm and hand kinematics. While this finding is seemingly in contradiction to the dual channels hypothesis, one possibility is that the hand representation in PMd is in the service of reaching and the arm representation in PMv is in the service of grasping. Thus, we explicitly tested if there is any preferential encoding of single unit activities of PMd and PMv neurons using functional representations of prehensile movements revealed by dPCA. Specifically, we fit encoding models using only reaching components, or only grasping components of the dPCA analysis. We found that both reach and grasp kinematic synergies predicted spiking activity in both PMd and PMv (Fig. 8A; Wilcoxon signed rank test, all $p < 0.01$).

Again, we performed a control analysis to verify that both reaching and grasping kinematic synergies were encoded in the spiking activity of premotor cortical cells. We assessed the extent to which a full model containing both reach and grasp synergies outperformed a model containing only reach, or only grasp (Fig. 8B). Here, we found

(Table 2) that 69% PMd and 56% PMv cells for monkey J and 93% PMd and 91% PMv cells for monkey L encoded reaching kinematics while 88% PMd and 65% PMv cells for monkey J and 97% PMd and 91% PMv cells for monkey L encoded grasping. The proportion of cells that simultaneously encoded both reach and grasp (monkey J: 67% PMd and 53% PMv cells and monkey L: PMd 90% PMd and 91% PMv cells respectively) was significantly more frequent than would be expected under chance if reach and grasp were independent (binomial test, $B_{0.628,\ 136} = 98$, $p < 0.01$). Although many cells encoded both reach and grasp simultaneously, subtracting the AUROC of the reach and grasp models revealed there was a preferential representation of reaching in the PMv of animal J and PMd of animal L because, as a population, the difference in AUROC between the reach only and grasp only models was significantly different from 0 (Fig. 8C, Wilcoxon signed rank test, J: $Z = 3.58$, $p < 0.01$; L: $Z = 3.75$, $p < 0.01$).

Finally, we considered the relationship between the anatomical and functional kinematic features encoded by each cell. To this end, we compared the difference of arm and hand model AUROCs to the difference of reach and grasp model AUROCs. Under the classical model, we might assume that PMd cells preferentially encode the kinematics of the arm and prefer the kinematics of reaching, and correspondingly, PMv cells prefer the hand and grasping (Fig. 9A). Such a simplistic relationship, however, does not appear to capture the patterns we observed in our data because we observed several cells that preferred both hand and reach or arm and grasp in both PMd and PMv (Fig. 9B). These results indicate that anatomical encoding preferences are not clearly related to functional encoding preferences as we failed to reject the null hypothesis that

functional and anatomical encoding preferences were statistically independent (chi-squared test of independence, X^2 with 1 d.f. = 3.03, $p > 0.05$).

We additionally considered the strength of anatomical and functional representations in each area. Specifically, we sought to ask if anatomical or functional relationships were more strongly encoded in a given area. To do so, we computed the logarithm of the ratio of the arm AUROC and reach AUROC (Fig. 9C), or the hand AUROC and the grasp AUROC (Fig. 9D). If this number is negative, that would indicate that functional kinematic synergies predict spiking activity better than the anatomical features; however, if this number is positive, then the anatomical features predict spiking activity better than functional kinematic synergies. In both PMd and PMv, we found that anatomical features were more strongly encoded as compared to functional synergies because the logs of AUROC ratios were positive (Wilcoxon signed rank test, all $p < 0.01$). However, the degree to which anatomical features were preferred differed between areas. We found that anatomical features were significantly more strongly represented in the activity of PMd cells as compared to PMv (Fig. 9C-D; Mann Whitney *U*-test, arm / reach: $Z = 3.87$, $p < 0.01$, hand / grasp: $Z = 2.64$, $p < 0.01$).

Encoding of intrinsic features in premotor cortex

Since extrinsic features were not the sole predictors of spiking activity, we also explored how intrinsic features are encoded in premotor cortex. We compared the encoding performance of the full kinematic model to the full intrinsic, i.e. spike history model. The spike-history model contained information about the spike histories of all other simultaneously recorded neurons at a variety of temporal scales (Fig. 10; see methods for details). We found that spike history was an effective predictor of spiking

activity (Fig. 10A; Wilcoxon signed rank test, animal J PMd: $W = 91$, $p < 0.01$; PMv: $W = 78$, $p < 0.01$; animal L PMd: $Z = 4.7$, $p < 0.01$ PMv: $Z = 4.1$, $p < 0.01$). In animal J, we found spike history predicted PMd activity significantly better than PMv (Mann-Whitney *U*-test, $Z = 2.20$, $p < 0.03$), but there was no difference in animal L across areas ($Z = -0.33$, $p > 0.05$). Also, spike history better predicted spiking activity than the kinematics in all areas (Fig. 10B, all Bonferroni corrected $p < 0.011$).

We wanted to identify which temporal scale of intrinsic activities led to the best encoding performance. We fit models using each of the three different temporal scales and found that the longest temporal scale (108 ms) led to the best encoding performance in both animals irrespective of cortical area (Fig. 10C). We subsequently wondered if the information at each temporal scale was totally redundant, or, if using spike history at multiple temporal scales led to superior predictive ability. Accordingly, we compared the AUROC at the best temporal scale for each cell and compared it to the AUROC of the full spike history model including all temporal scales (Fig. 10D). In the PMd of animal J, we observed that there was no significant difference between the AUROC of the full spike history model and the model at the best lag (Wilcoxon rank sum test, PMd: $W = 69$, $p < 0.11$). In contrast, spike history at multiple spatial scales better predicted spiking activity in the PMv of both animals (J: $W = 69$, $p < 0.02$, L: $Z = 4.11$, $p < 0.01$) and the PMd of animal L ($Z = 3.30$, $p < 0.01$).

Discussion

Demixed principal component analysis

Here, we applied a novel dimensionality reduction technique, demixed principal component analysis (Kobak et al., 2016), to identify kinematic synergies associated with either reaching or grasping during an unconstrained prehensile movement task. In both animals, we observed that a few functionally defined kinematic synergies accounted for most of the variance in the data. Moreover, reaching and grasping synergies each was explained a large proportion of the kinematic variance. In contrast, comparatively little variance was due to interactions between reaching and grasping conditions, supporting the decomposition of kinematics into reaching and grasping sub-movements (Jeannerod, 1984; Haggard and Wing, 1995).

Although this method provides a promising avenue for gaining insight into prehensile movements, there are some limitations to the approach. Chiefly, the relationship between the demixed kinematic synergies and muscle synergies currently remains unknown. Using a similar approach to our current method, instantaneous lengths of 50 musculotendon units were estimated, and it was found that 8 PCA components were sufficient to explain more than 95% of variance while at least 11 components were needed in the joint angle space to capture the same amount of variance for monkeys performing reach-to-grasp (Schaffelhofer et al., 2015). Recent work has argued that the encoding preferences of primary motor cortical neurons reflect muscle synergies evoked by intracortical microstimulation (Overduin et al., 2014). In complementary work, it was demonstrated that decoding joint kinematics from units on electrodes that evoked movements of that joint when stimulated led to better decoding performance as compared to a simple random allocation (Best et al., 2014). The kinematic synergies identified by dPCA, however, arose from our experimental design.

In future work, we wish to address the similarity between kinematic synergies inferred using dPCA, and kinematic or muscle synergies characterized via ICMS.

At a more technical level, dPCA is limited in that it is based on trial-averaged data and fails to account for trial-to-trial variation within an experimental condition. An additional limitation is that it does not support the use of continuous variables as conditions. That is, object locations were not treated as positions in Euclidean space, but rather discrete covariates. Finally, on individual trials, the scores of the dPCs often exhibited strong moment-by-moment correlations suggesting that even though reach and grasp were decoupled across conditions, within a condition there may remain some strong correlation.

Implications for cortical control of reach to grasp

Here, we used GLMs to develop encoding models of spiking activity in premotor cortex based on intrinsic and extrinsic features. We found evidence that challenges the dogmatic view of premotor cortical organization centered around discrete reaching (dorsomedial) and grasping (dorsolateral) pathways. In particular, we demonstrated that there was a complete anatomical representation of the upper limb in PMd. This finding is consistent with previous studies that used intracortical-microstimulation to study motoric representations in PMd and further work that showed firing rates of PMd neurons are modulated by changes in grasping condition (Raos et al., 2003, 2004; Fattori et al., 2010). Additional work has demonstrated that whole arm kinematics can be decoded from PMd ensemble activity (Bansal et al., 2012). Our work complements that study by showing that single cells encode complex, whole-arm kinematics. Furthermore, our finding is consistent with studies on single units from area V6A, which

522 is a part of the dorsomedial reaching network, illustrating that the dorsomedial pathway
523 is also involved in hand preshaping and grip formation and may play a central role for all
524 phases of reach-to-grasp movements (Fattori et al., 2010, 2012). Similarly, in PMv, we
525 also found a complete representation of the upper limb, although, in absolute terms, it
526 was weaker than in PMd. This result is consistent with previous reports that ICMS of
527 PMv occasionally evoked arm movements (Godschalk et al., 1981, 1985; Hocherman
528 and Wise, 1991; Stark et al., 2007).

529 Kinematically, we demonstrated that arm kinematics were affected by grasping
530 condition and hand kinematics were affected by reaching condition, so, while we
531 demonstrated that whole arm representations were present in both PMd and PMv, that
532 was insufficient to argue against our null hypothesis that reach and grasp were
533 processed in independent pathways. We used a novel dimensionality reduction
534 technique to dissociate reaching from grasping and found that single neurons in PMd
535 and PMv encoded both reaching and grasping kinematic synergies. Moreover, across
536 the entire population of recorded cells, we found no relationship between anatomical
537 and functional representations. That is, the anatomical preferences of a cell (i.e.
538 whether it was biased towards arm or hand kinematics) were not related to its functional
539 preferences (i.e. whether it preferred reach or grasp synergies).

540 *Differences between PMd and PMv*

541 In this work, we compared the encoding properties of neurons simultaneously
542 recorded in the dorsal and ventral premotor cortex of two rhesus macaques. By using
543 this simultaneous recording paradigm, our results were not confounded by potential
544 behavioral differences across sessions.

In both animals, we observed that movement kinematics was more strongly represented in PMd as compared to PMv. One potential explanation for this finding is that PMd is seemingly more directly related to motor output. Pyramidal cells in layer V of PMd comprise approximately 10% of fibers from the frontal lobe in the corticospinal tract (Dum and Strick, 1991), and intracortical microstimulation of PMd is known to elicit arm movements (Weinrich and Wise, 1982; Weinrich et al., 1984). Consistent with this interpretation, we found that spiking activity in PMd was generally better predicted by anatomical features rather than functional kinematic synergies. PMv too sends projections to spinal cord, but it largely projects to the upper cervical spinal segments (He et al., 1993). Recent work using ICMS has shown that PMv acts on spinal cord primarily through facilitation of MI (Cerri et al., 2003; Shimazu et al., 2004).

In both animals, we observed that while single cells in PMd encode whole arm kinematics, they exhibit a preferential encoding of arm kinematics. This is consistent with the classical studies of PMd implicating it in the control of reaching movements (Weinrich and Wise, 1982; Weinrich et al., 1984; Kurata and Tanji, 1986; Riehle and Requin, 1989; Pesaran et al., 2006).

In PMv, however, we observed no consistent bias for either arm or hand kinematics or grasp or reach kinematics despite some studies illustrated causal influence of PMv lesion to a grasp deficit (Fogassi et al., 2001). Additionally, in PMv, we found that spike history at multiple time scales was a better predictor of spiking activity than a single timescale. This suggests that PMv may be more influenced by several internal processes operating at different timescales, and may also explain why kinematics was not strongly represented in PMv. An alternative possibility is that these

568 types of unconstrained movements are not the most effective drivers of activity in PMv,
569 but rather a different class of movement altogether may be represented (Wise, 2006;
570 Lehmann and Scherberger, 2013; Bonini et al., 2014). It should be noted that the PMv
571 arrays were placed on or close to the convexity of the inferior arm of arcuate sulcus.
572 Thus, we were not sampling from neurons in the sulcus, particularly F5p, and were
573 likely recording from neurons in F4 as well as F5 divisions of PMv (Matelli et al., 1985).
574
575 *Inter-animal differences*
576 We observed some differences in behavior between the two animals. Animal J
577 had faster reaction times than animal L, and, generally, executed faster movements that
578 were qualitatively more stereotyped. Although the movements were executed at
579 different speeds and with different reaction times, we observed many similarities in the
580 dPCA analysis across the two animals suggesting that the kinematic synergies we
581 identified were robust across a naturalistic range of self-selected movement speeds. In
582 future work, it could be tested if the same set of dPCA synergies predicts movement
583 kinematics at a variety of speeds by having an animal engage in a reach-to-grasp task
584 with an explicit speed cue.
585 An additional difference in the kinematics between the two animals was their
586 resting posture. In animal L, resting grasp aperture was proportionately much larger
587 than in animal J. Indeed, the grasp aperture was maximal at the rest position for some
588 trials in animal L. In contrast, animal J maintained a more closed aperture during the
589 rest epoch. This finding may explain why the temporal profiles of the largest dPC in
590 each animal are different. The temporal profile of the largest condition independent (CI)

591 dPC in animal J was a bell-shaped curve, reflecting that the hand opened and closed
592 during the reach to grasp movement. In contrast, the temporal profile of the largest CI
593 dPC in animal L was a sigmoidal curve corresponding to the fact that his hand started
594 opened and gradually conformed to the shape of the object to be grasped. Finally, the
595 animals adopted qualitatively different strategies to successfully grasp the ring object.
596 Grasp aperture of the ring object in animal J followed a biphasic profile that was absent
597 in animal L.

598 At the neural level, there were also several differences between the two animals.
599 We observed that arm (as compared to hand) kinematics was preferentially represented
600 in PMv of animal J, but not L. One potential explanation of this finding is based on array
601 placement. Although an attempt was made to place the arrays in approximately the
602 same location in both animals, a large blood vessel constrained our placement of the
603 PMv array in animal J. In both animals, we saw a preferential representation of the arm
604 in PMd. However, animal J's PMv array was inserted much closer to its PMd array
605 because of the aforementioned blood vessel as compared to animal L. Accordingly, the
606 arm representation in the PMv of J may be stronger because it is closer to PMd.

607 In summary, we employed GLM framework to characterize encoding properties
608 of single neurons in PMd and PMv with kinematic inputs that were computed using a
609 novel dimensionality reduction technique (dPCA) to dissociate anatomical
610 representations of arm and hand from functional representations of reach and grasp.
611 We showed that kinematics was more prominently encoded in PMd responses as
612 compared to PMv. More importantly, there was no consistent preference for arm versus
613 hand or for reach versus grasp kinematics in either PMd or PMv. By considering the

614 encoding of kinematic trajectories, our findings extend but are consistent with the results
615 in a previous study (Stark and Abeles, 2007) that demonstrated that the encoding
616 properties of PMd and PMv neurons often show mixing between reach and grasp which
617 suggests that these two cortical areas may functionally serve as a neural substrate for
618 coordination between reach and grasp during prehension.
619
620
621
622
623

624 **References**

625 Bansal AK, Truccolo W, Vargas-Irwin CE, Donoghue JP (2012) Decoding 3D reach and
626 grasp from hybrid signals in motor and premotor cortices: spikes, multiunit activity,
627 and local field potentials. J Neurophysiol 107:1337–1355.
628 Best MD, Suminski AJ, Takahashi K, Hatsopoulos NG (2014) Consideration of the
629 functional relationship between cortex and motor periphery improves offline
630 decoding performance. 2014 36th Annu Int Conf IEEE Eng Med Biol Soc:4868–
631 4871.
632 Bonini L, Maranesi M, Livi A, Fogassi L, Rizzolatti G (2014) Space-Dependent
633 Representation of Objects and Other's Action in Monkey Ventral Premotor
634 Grasping Neurons. J Neurosci 34:4108–4119.
635 Borra E, Belmalih A, Calzavara R, Gerbella M, Murata A, Rozzi S, Luppino G (2008)
636 Cortical Connections of the Macaque Anterior Intraparietal (AIP) Area. Cereb

637 Cortex 18:1094–1111.
638 Brendel W, Romo R, Machens CK (2011) Demixed Principal Component Analysis. In:
639 Advances in Neural Information Processing Systems 24 (Shawe-Taylor J, Zemel
640 RS, Bartlett PL, Pereira F, Weinberger KQ, eds), pp 2654–2662. Curran
641 Associates, Inc.
642 Cerri G, Shimazu H, Maier MA, Lemon RN (2003) Facilitation from ventral premotor
643 cortex of primary motor cortex outputs to macaque hand muscles. J Neurophysiol
644 90:832–842.
645 Dea M, Hamadjida A, Elgbeili G, Quessy S, Dancause N (2016) Different Patterns of
646 Cortical Inputs to Subregions of the Primary Motor Cortex Hand Representation in
647 *Cebus apella*. Cereb Cortex 1:bhv324.
648 Delp SL, Anderson FC, Arnold AS, Loan P, Habib A, John CT, Guendelman E, Thelen
649 DG (2007) OpenSim: Open-Source Software to Create and Analyze Dynamic
650 Simulations of Movement. IEEE Trans Biomed Eng 54:1940–1950.
651 Dum RP, Strick PL (1991) The origin of corticospinal projections from the premotor
652 areas in the frontal lobe. J Neurosci 11:667–689.
653 Dum RP, Strick PL (2005) Frontal lobe inputs to the digit representations of the motor
654 areas on the lateral surface of the hemisphere. JNeurosci 25:1375–1386.
655 Fattori P, Breveglieri R, Amoroso K, Galletti C (2004) Evidence for both reaching and
656 grasping activity in the medial parieto-occipital cortex of the macaque. Eur J
657 Neurosci 20:2457–2466.
658 Fattori P, Breveglieri R, Raos V, Bosco A, Galletti C (2012) Vision for action in the
659 macaque medial posterior parietal cortex. J Neurosci 32:3221–3234.

660 Fattori P, Raos V, Breveglieri R, Bosco A, Marzocchi N, Galletti C (2010) The
661 dorsomedial pathway is not just for reaching: grasping neurons in the medial
662 parieto-occipital cortex of the macaque monkey. J Neurosci 30:342–349.
663 Fogassi L, Gallese V, Buccino G, Craighero L, Fadiga L, Rizzolatti G (2001) Cortical
664 mechanism for the visual guidance of hand grasping movements in the monkey: A
665 reversible inactivation study. Brain 124:571–586.
666 Godschalk M, Lemon RN, Kuypers HG, van der Steen J (1985) The involvement of
667 monkey premotor cortex neurones in preparation of visually cued arm movements.
668 Behav Brain Res 18:143–157.
669 Godschalk M, Lemon RN, Nijs HGT, Kuypers HGJM (1981) Behaviour of neurons in
670 Monkey peri-arcuate and precentral cortex before and during visually guided arm
671 and hand movements. Exp Brain Res 44789:113–116.
672 Grafton ST (2010) The cognitive neuroscience of prehension: Recent developments.
673 Exp Brain Res 204:475–491.
674 Haggard P, Wing A (1995) Coordinated responses following mechanical perturbation of
675 the arm during prehension. Exp Brain Res 102:483–494.
676 Hatsopoulos NG, Xu Q, Amit Y (2007) Encoding of movement fragments in the motor
677 cortex. J Neurosci 27:5105–5114.
678 He SQ, Dum RP, Strick PL (1993) Topographic organization of corticospinal projections
679 from the frontal lobe: motor areas on the lateral surface of the hemisphere. J
680 Neurosci 13:952–980.
681 Hocherman S, Wise SP (1991) Effects of hand movement path on motor cortical activity
682 in awake, behaving rhesus monkeys. Exp Brain Res 83678:285–302.

683 Hoshi E, Tanji J (2007) Distinctions between dorsal and ventral premotor areas:
684 anatomical connectivity and functional properties. Curr Opin Neurobiol 17:234–242.
685 Jeannerod M (1984) The timing of natural prehension movements. J Mot Behav
686 16:235–254.
687 Jeannerod M (1988) The neural and behavioural organization of goal-directed
688 movements. Oxford: Oxford Science Publications.
689 Kaas JH, Gharbawie OA, Stepniewska I (2013) Cortical networks for ethologically
690 relevant behaviors in primates. Am J Primatol 75:407–414.
691 Karl JM, Whishaw IQ (2013) Different evolutionary origins for the Reach and the Grasp:
692 An explanation for dual visuomotor channels in primate parietofrontal cortex. Front
693 Neurol 4 DEC:1–13.
694 Kobak D, Brendel W, Constantinidis C, Feierstein CE, Kepecs A, Mainen ZF, Romo R,
695 Qi X, Uchida N, Machens CK (2016) Demixed principal component analysis of
696 neural population data. Elife 5:1–37.
697 Kurata K, Tanji J (1986) Premotor cortex neurons in macaques: activity before distal
698 and proximal forelimb movements. J Neurosci 6:403–411.
699 Lehmann SJ, Scherberger H (2013) Reach and Gaze Representations in Macaque
700 Parietal and Premotor Grasp Areas. J Neurosci 33:7038–7049.
701 Luppino G, Murata A, Govoni P, Matelli M (1999) Largely segregated parietofrontal
702 connections linking rostral intraparietal cortex (areas AIP and VIP) and the ventral
703 premotor cortex (areas F5 and F4). Exp Brain Res 128:181–187.
704 Mason CR, Gomez JE, Ebner TJ (2001) Hand synergies during reach-to-grasp. J
705 Neurophysiol 86:2896–2910.

706 Matelli M, Luppino G, Rizzolatti G (1985) Patterns of cytochrome oxidase activity in the
707 frontal agranular cortex of the macaque monkey. Behav Brain Res 18:125–136.
708 Mollazadeh M, Aggarwal V, Davidson AG, Law AJ, Thakor N V., Schieber MH (2011)
709 Spatiotemporal variation of multiple neurophysiological signals in the primary motor
710 cortex during dexterous reach-to-grasp movements. J Neurosci 31:15531–15543.
711 Mollazadeh M, Aggarwal V, Thakor N V, Schieber MH (2014) Principal components of
712 hand kinematics and neurophysiological signals in motor cortex during reach to
713 grasp movements. J Neurophysiol:1857–1870.
714 Overduin S a, d'Avella A, Carmena JM, Bizzi E (2014) Muscle synergies evoked by
715 microstimulation are preferentially encoded during behavior. Front Comput
716 Neurosci 8:20.
717 Pesaran B, Nelson MJ, Andersen RA (2006) Dorsal Premotor Neurons Encode the
718 Relative Position of the Hand, Eye, and Goal during Reach Planning. Neuron
719 51:125–134.
720 Raos V, Franchi G, Gallese V, Fogassi L (2003) Somatotopic organization of the lateral
721 part of area F2 (dorsal premotor cortex) of the macaque monkey. J Neurophysiol
722 89:1503–1518.
723 Raos V, Umilta MA, Gallese V, Fogassi L, Umiltá M-A (2004) Functional properties of
724 grasping-related neurons in the dorsal premotor area F2 of the macaque monkey. J
725 Neurophysiol 92:1990–2002.
726 Riehle A, Requin J (1989) Monkey primary motor and premotor cortex: single-cell
727 activity related to prior information about direction and extent of an intended
728 movement. J Neurophysiol 61:534–549.

729 Saleh M, Takahashi K, Amit Y, Hatsopoulos NG (2010) Encoding of coordinated grasp
730 trajectories in primary motor cortex. J Neurosci 30:17079–17090.
731 Saleh M, Takahashi K, Hatsopoulos NG (2012) Encoding of coordinated reach and
732 grasp trajectories in primary motor cortex. J Neurosci 32:1220–1232.
733 Santello M, Soechting JF (1998) Gradual Molding of the Hand to Object Contours. J
734 Neurophysiol 79:1307–1320.
735 Schaffelhofer S, Sartori M, Scherberger H, Farina D (2015) Musculoskeletal
736 Representation of a Large Repertoire of Hand Grasping Actions in Primates. IEEE
737 Trans Neural Syst Rehabil Eng 23:210–220.
738 Shimazu H, Maier MA, Cerri G, Kirkwood PA, Lemon RN (2004) Macaque ventral
739 premotor cortex exerts powerful facilitation of motor cortex outputs to upper limb
740 motoneurons. J Neurosci 24:1200–1211.
741 Stark E, Asher I, Abeles M (2007) Encoding of Reach and Grasp by Single Neurons in
742 Premotor Cortex Is Independent of Recording Site. J Neurophysiol 97:3351–3364.
743 Todorov E, Ghahramani Z (2004) Analysis of the synergies underlying complex hand
744 manipulation. In: 26th Annual International Conference of the IEEE Engineering in
745 Medicine and Biology Society, 2004. IEMBS ’04, pp 4637–4640.
746 Truccolo W, Hochberg LR, Donoghue JP (2010) Collective dynamics in human and
747 monkey sensorimotor cortex: predicting single neuron spikes. Nat Neurosci
748 13:105–111.
749 Weinrich M, Wise SP (1982) The premotor cortex of the monkey. J Neurosci 2:1329–
750 1345.
751 Weinrich M, Wise SP, Mauritz K-H (1984) A Neurophysiological Study of the Premotor

Cortex in the Rhesus Monkey. Brain 107:385–414.

Wise SP (2006) The ventral premotor cortex, corticospinal region C, and the origin of primates. Cortex 42:521–524.

Figure Legends

Figure 1 Methods. A. Animals were trained to grasp a variety of geometric shapes including (left to right) ring (vertical), small disc (out), key, small Disc (horizontal), cylinder (horizontal). These drawings depict static hand conformation during grasping of these objects. **B**. Target locations in relation to the starting position. Aerial view (Top) and side view (bottom). Blue circle denotes the starting position and white circles denote target locations respectively. Red numbers in or near the target circles indicate the location numbers, 1-4. **C.** Drawing of animal J in rest position. Pink dots correspond

to the approximate placement of the infrared markers. **D.** Depiction of the arm in the same position as **C.** in the Opensim software environment. **E-F.** Placement of electrode arrays in animals L and J, respectively.

Figure 2 Trial-averaged kinematics of the arm, wrist and hand. A. Within-condition trial-averaged kinematics for three degrees of freedom in the arm (left column), wrist (center column) and hand (right column) of animal J. Line style indicates object location while color indicates grip types. **B.** We found that the object can significantly affect arm kinematics (top). Here, we computed the average humerus abduction over all object locations when grasping Cyl o (purple trace) and Ring h (green trace). Shaded area indicates +- 2 standard errors of the mean (S.E.M.) Similarly, reach location can affect hand kinematics (bottom). Flexion in the metacarpophalangeal joint of the second digit (2mcp flexion) was averaged over all objects and is shown for two object locations. **C.** We computed the grasp aperture, defined as the distance between the distal-most thumb and index finger markers and plotted it relative to movement onset in both animals.

Figure 3 Demixed principal component analysis. A. Scree plot of demixed PCA. The cumulative percentage of explained variance for a given number of dPCs is shown for joint angles. Each individual component varies only along one task parameter. It can be either reach related (R, red points), grasp related (G, green points), condition independent (CI, gold points), or an interaction between reach and grasp condition (I, blue points). Marker shape (either square or triangle) indicates animal. Note that the scree plots are highly similar across animals. **B.** Percentage of variance explained by the different task conditions in joint angle data. **C.** Visualization of kinematic synergies revealed by the demixed PCA. The posture of the upper limb is shown at various projections along the largest condition independent synergy (top row), the largest grasp synergy (middle row), and the largest reach synergy (bottom row). Data are from animal J.

Figure 4 Trial averaged dPCA trajectories relative to movement onset. The temporal profile of the first four dPCs is shown for the various object locations and grips. Conventions are the same as Fig. 2. To the left of each dPC is an indication of whether it is a condition-independent (CI), grasp (G), or reach (R). The components are ordered from top to bottom in terms of variance explained; that is, dPC1 explained more variance than all others.

Figure 5 Exemplary single unit spiking activities of neurons in PMd (A) and PMv (B) for monkey L reaching to grasp different objects at different locations. Each raster plot corresponds to a particular object and location combination while each PSTH was computed for either one object over all locations or one location over all objects. Time 0 corresponds to movement onset.

Figure 6 Encoding models that include kinematics predict spiking activity better than set-related models. A. We fit encoding models using either set-related activity or kinematics to each neuron in our sample and measured the area under the receiver

operating characteristic curve (AUROC) across 10 folds of cross validated data. Here, each point corresponds to the median AUROC across folds as a function of animal (triangles or squares) and model type. Cells in PMd are blue, while cells in PMv are red. The vertical line next to each point-set indicates the interquartile range while the median is indicated with the horizontal line. **B.** Distribution of differences between kinematic and set-related models. The lines to the immediate right of each point-set follow the same conventions as **A.** Kinematic models predicted spiking activity better than set-related activity models in PMd and PMv in both animals (significance codes: *** $p < 0.0005$, see main text for additional statistics).

Figure 7 Comparing encoding performance of models based on an anatomical division of the upper limb. A. We fit GLMs using either arm or hand (including wrist) kinematics. For each model type and animal, the distribution of median AUROCs across folds is shown as raw data (left column; each point corresponds to a cell) and interquartile range + median (vertical and horizontal lines, respectively). **B.** Median AUROCs were compared between the full model that included all kinematic terms, and reduced models that contained only arm, or only hand kinematics. **C**. Distribution of differences in arm and hand AUROCs. We found that arm kinematics were preferentially encoded by PMd in both animals and also in PMv in animal J because a significant proportion of cells preferred arm kinematics in those two areas (significance codes: * $p < 0.05$, ** $p < 0.005$; see main text for additional statistics).

Figure 8 Comparing encoding performance of models based on a functional division of the upper limb. A. We fit GLMs using either reach or grasp kinematic synergies. For each model type and animal, the distribution of median AUROCs across folds is shown as raw data (left column) and interquartile range + median (vertical and horizontal lines, respectively). **B.** Median AUROCs were compared between the full model that included both reach and grasp synergies, and reduced models that contained only reach or only grasp synergies. **C**. Distribution of differences in reach and grasp AUROCs. We found that reach kinematic synergies were preferentially encoded by PMv in animal J and PMd in animal L (significance codes: *** $p < 0.0005$ see text for additional statistics).

Figure 9 Comparing anatomical and functional representations in premotor cortex. We compared the differences of arm and hand AUROCs to the differences of reach and grasp AUROCs to determine if there was a systematic relationship such that cells that preferentially encoded arm kinematics likewise encoded reaching synergies, and similarly, cells that preferentially encoded hand kinematics likewise encoded grasping synergies. **A.** Expected results based on the dual channels hypothesis. PMd would be concerned exclusively with arm kinematics and reaching, while PMv would be concerned with hand kinematics and grasping. There would be a segregation of both function and anatomy between PMd and PMv. **B.** Actual results based on observed data. A chi-squared test of independence revealed no significant relationship between functional and anatomical encoding preferences. **C.** Comparing the relative encoding performance of anatomical and functional models. Here, we show the distribution of the logarithm of the ratio of arm and reach model AUROCs. If the log of this ratio is positive, then the arm model had a higher AUROC than the reach model, and vice versa for negative values. We found that both PMd and PMv are better predicted by

anatomical features rather than functional features, but this preference is stronger in PMd (see main text for additional statistics). **D.** Same conventions as panel **C**. but using hand and grasp models.

Figure 10 Encoding properties of intrinsic features and comparing spike history with kinematics in premotor cortex. A. We found that spike history from all cells at multiple temporal scales effectively predicted spiking activity (see main text for statistics). Each point corresponds to a cell from a given animal (shape) and cortical area (color). Lines next to each column of data indicate interquartile range and median. **B.** We compared the performance of the spike history model to the full kinematic model and observed that generally, spike history was a more effective predictor of spiking activity than kinematics. **C.** Median AUROC across cross validation folds as a function of basis function, cortical area, and animal. In both areas, the longest spike history term had the best encoding performance. **D.** Distribution of the differences in AUROC between the full spike history model and a model based on the best single basis function (lag). To the right of each data column are the median and interquartile ranges of the data.

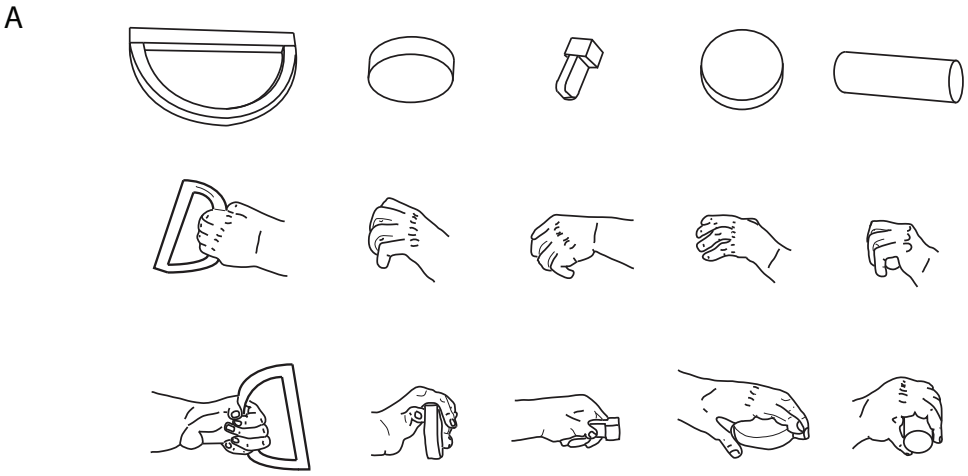

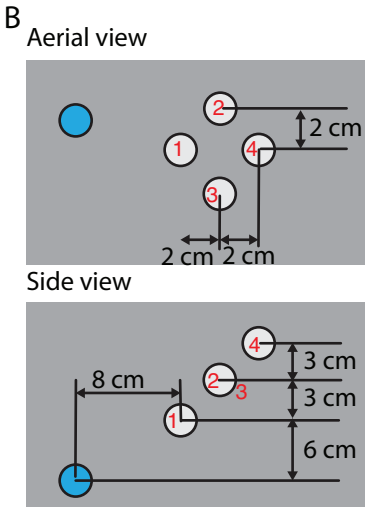

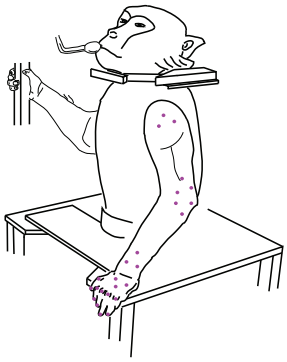

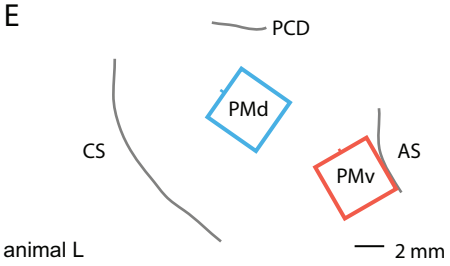

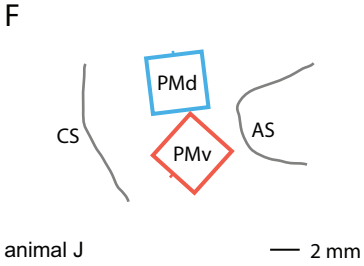

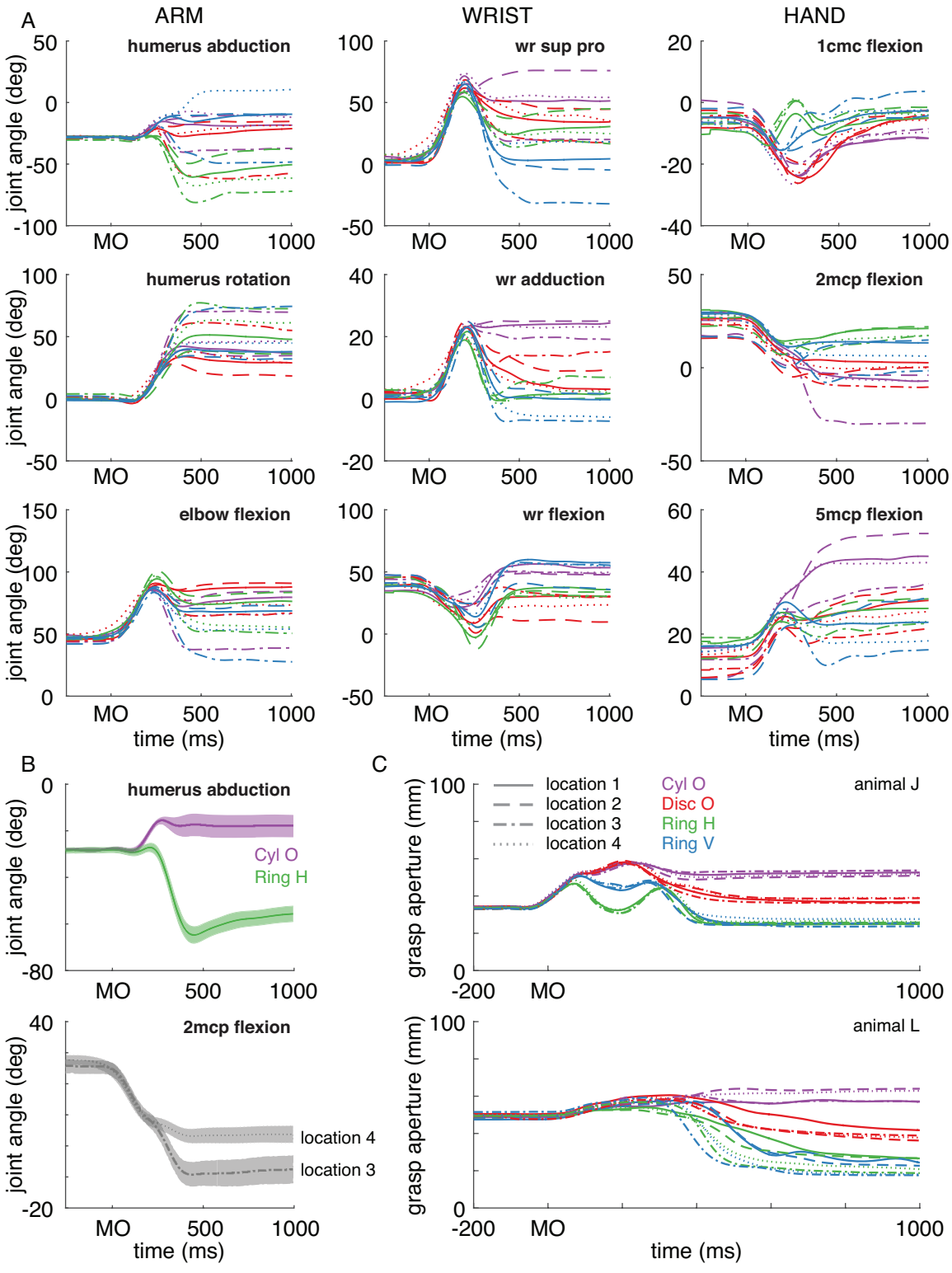

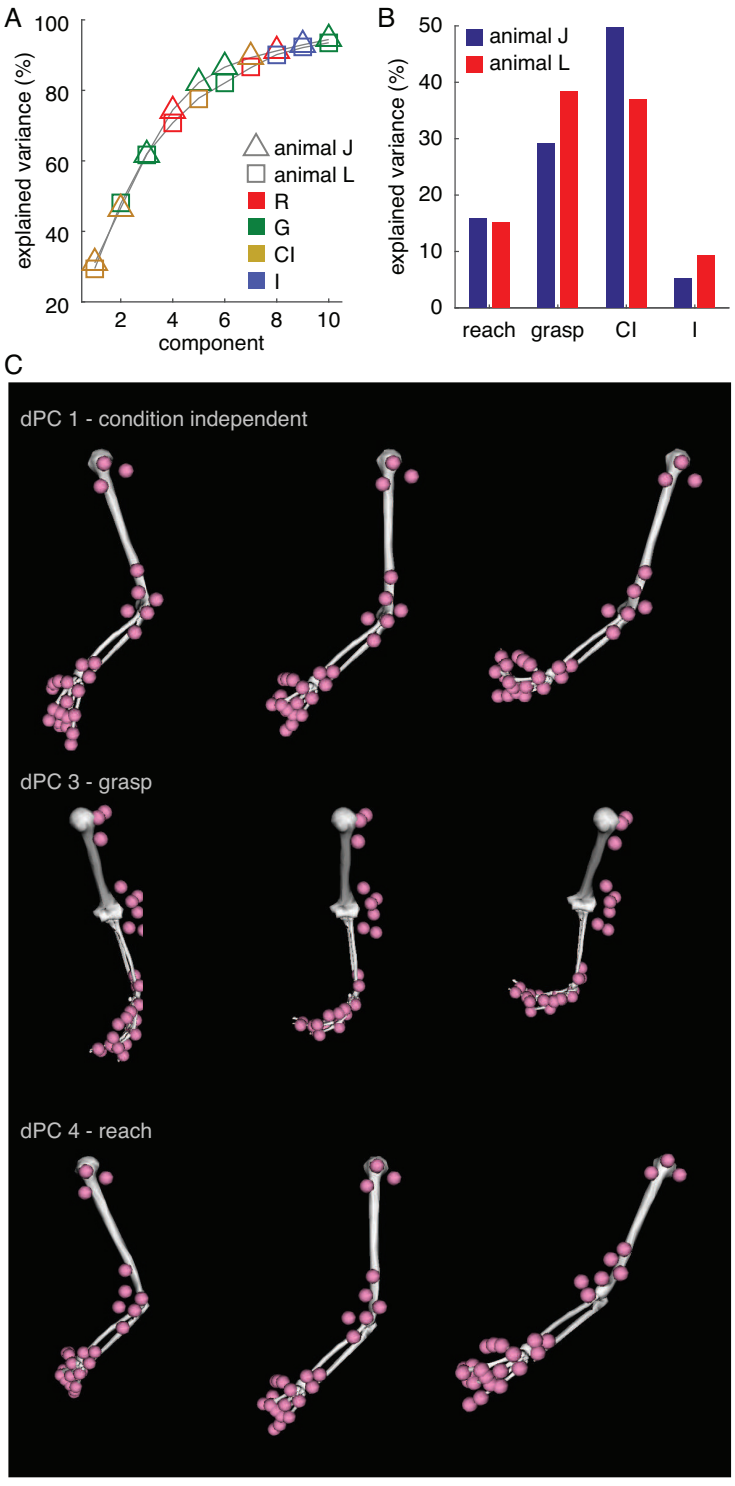

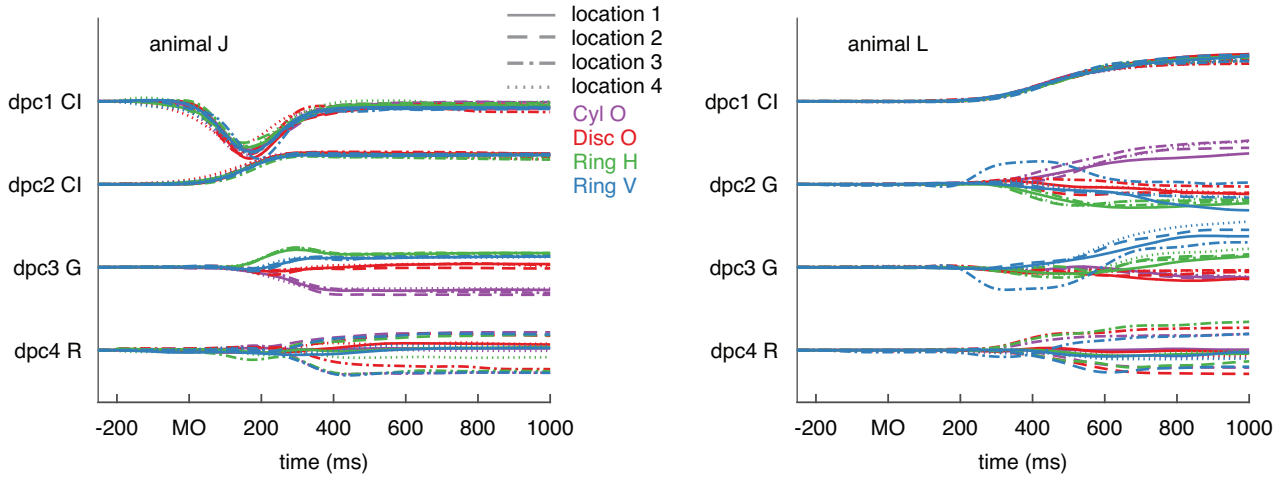

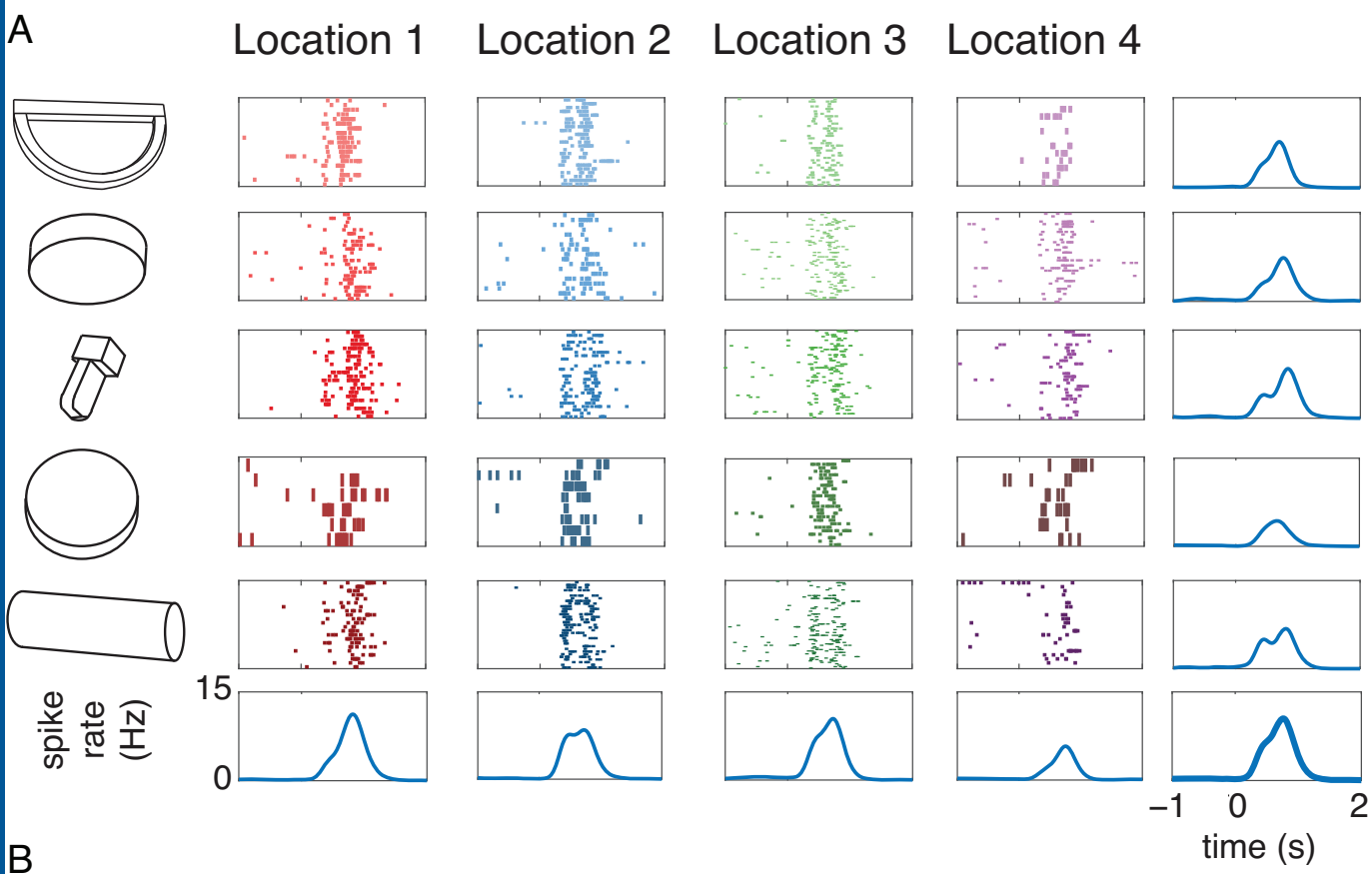

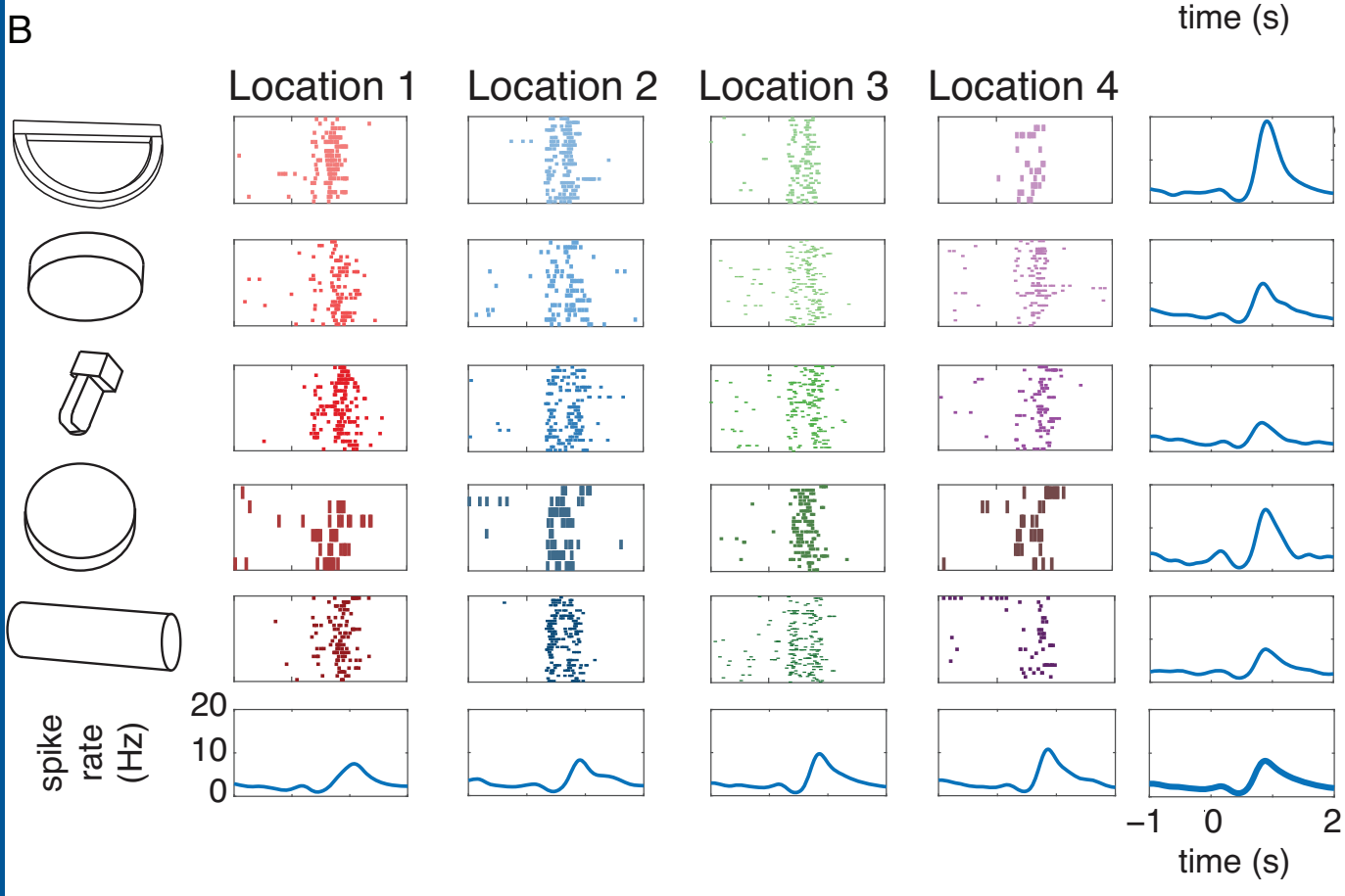

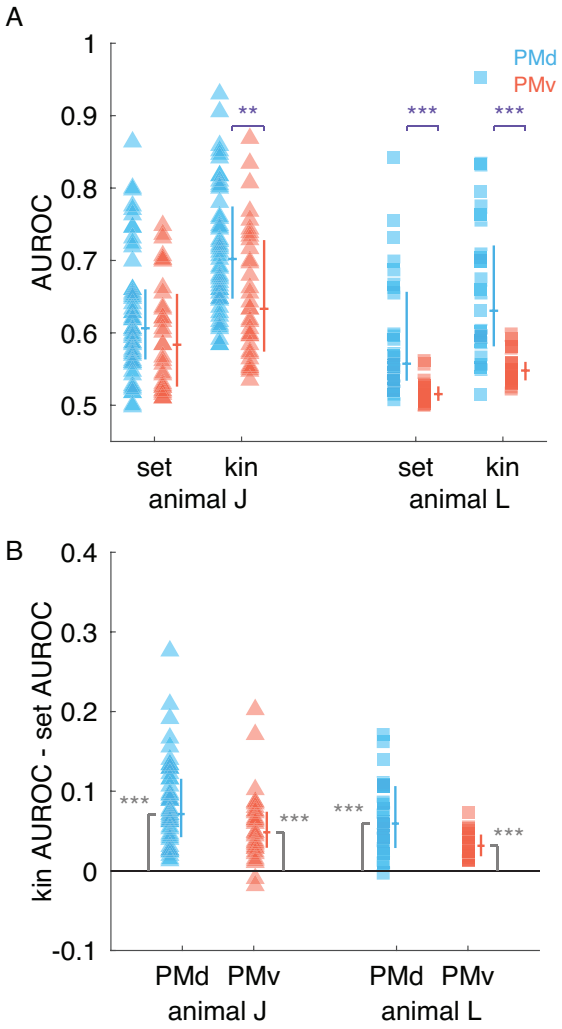

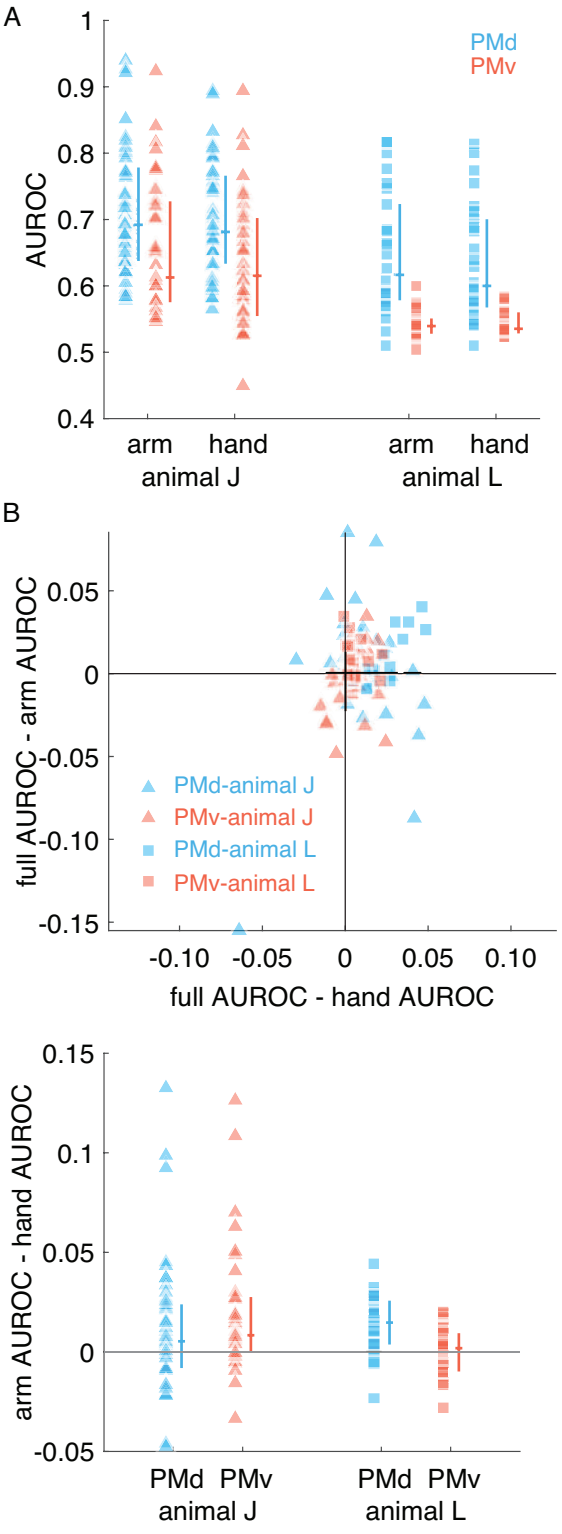

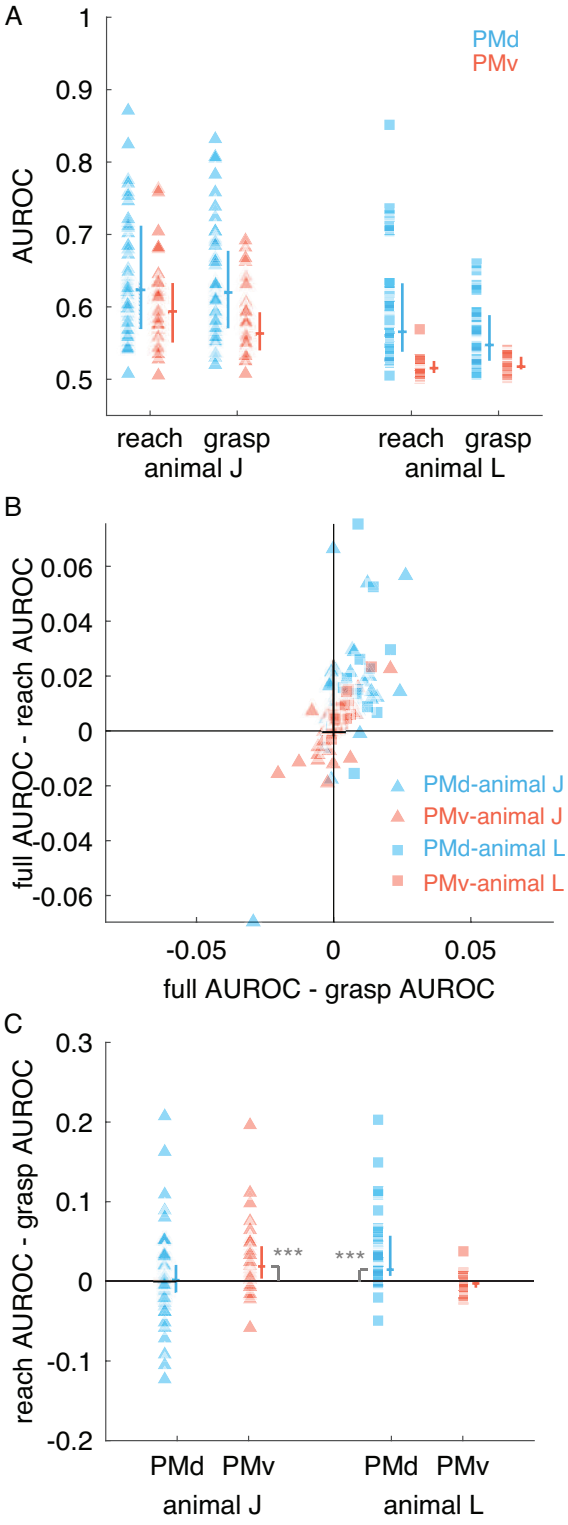

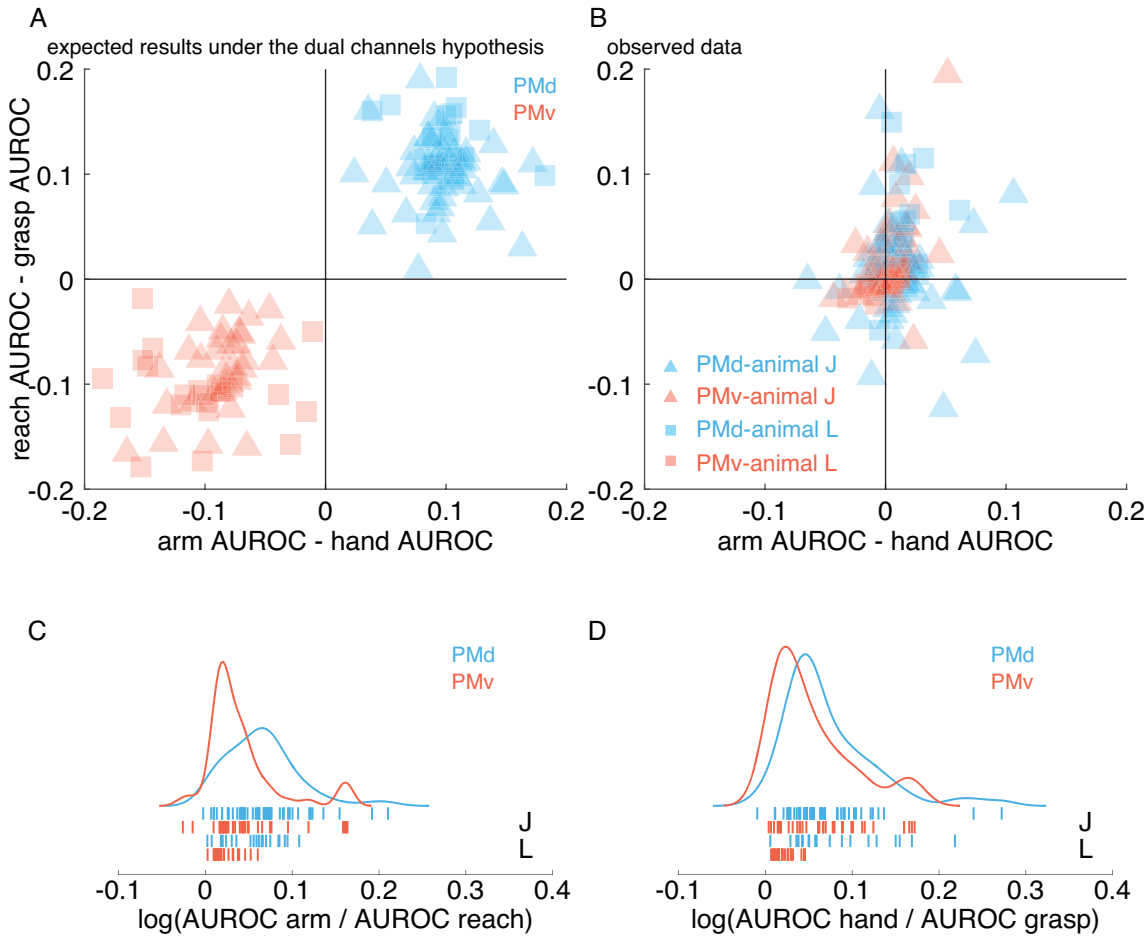

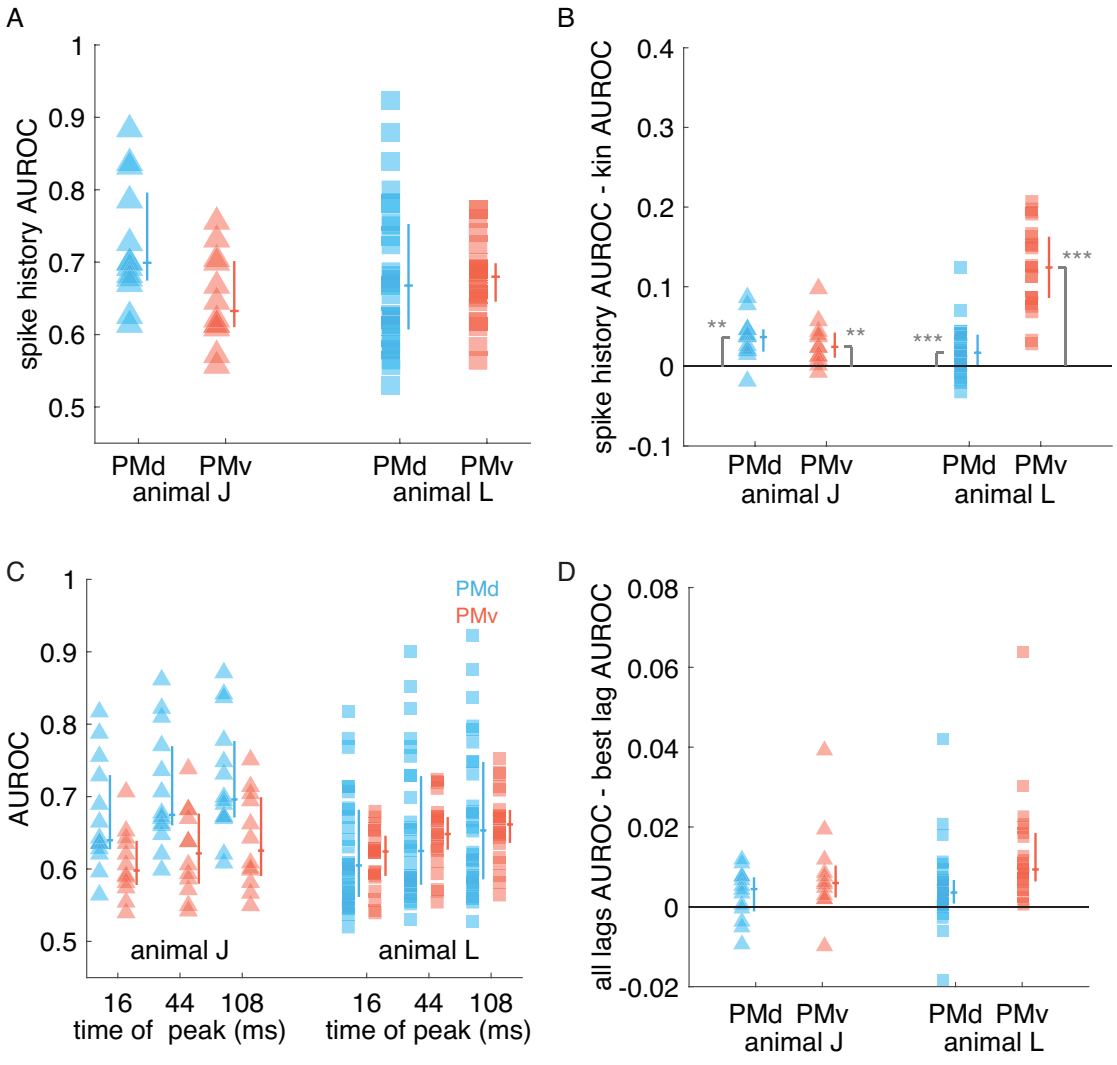

Tables

	PMd		PMv	
	animal J	animal L	animal J	animal L
Arm	82% (41/50)	100% (16/16)	79% (27/34)	95% (20/21)
Hand	56% (28/50)	75% (12/16)	53% (18/34)	76% (16/21)
Arm+Hand	42% (21/50)	75% (12/16)	41% (14/34)	71% (15/21)

Table 1. Percentage (number of neurons/total number) of neurons encoding arm, hand, or both arm & hand kinematics by area and animal.

	PMd		PMv	
	animal J	animal L	animal J	animal L
Reaching	69% (35/51)	93% (27/29)	56% (19/34)	91% (20/22)
Grasping	88% (45/51)	97% (28/29)	65% (22/34)	91% (20/22)
Reaching+Grasping	67% (34/51)	90% (26/29)	53% (18/34)	91% (20/22)

Table 2. Percentage (number of neurons/total number) of neurons encoding reaching, grasping, or both reaching & grasping kinematics by area and animal.